# Synthesis and Characterization of Polylactic Acid (PLA)-Coated $Fe_3O_4$@CQD Nanocomposites

Astuti*[1], Mulda Muldarisnur[1], Imelda[2], and Syafitri Rahmadhani[1]
[1]Physics Department
[2]Chemistry Department
Andalas University
Padang, 25163, West Sumatra, Indonesia
*astuti@sci.unand.ac.id*

Date received: September 12, 2025
Revision accepted: February 18, 2026

## Abstract

*This study aims to coat $Fe_3O_4$@CQD nanocomposites with polylactic acid (PLA) and investigate the effects of PLA concentration on their physicochemical properties, particularly fluorescence intensity and zeta potential. The results showed that PLA coating effectively increased luminescence intensity. After PLA coating, the fluorescence intensity increased dramatically, indicating reduced quenching. The results of the study show that the maximum fluorescence intensity is achieved at a PLA concentration of 2%. The sample with 2% PLA also shows a zeta potential of −32.2 mV, which is considered a relatively good colloidal stability by the widely accepted criterion of $|\zeta| \geq 30$ mV. SEM analysis reveals particle agglomeration, indicating that the coating does not entirely prevent aggregation. The 2% PLA formulation, therefore, shows promising physicochemical characteristics and may serve as a candidate for further investigation in bioimaging-related applications. Further biological studies are required to evaluate its biocompatibility and actual suitability for biomedical applications.*

***Keywords**:* $Fe_3O_4$@CQD, fluorescence, nanocomposite, polylactic acid, zeta potential

## 1. Introduction

New materials with magnetic and optical properties suitable for bioimaging for disease detection and treatment are created by combining magnetic and luminescent materials (Astuti *et al*., 2023, 2024; Wang & Deng, 2022). Biocompatibility, biodegradability, low toxicity, and high water dispersibility (with high stability) are all crucial properties of a bioimaging substance. $Fe_3O_4$@CQD nanocomposite is an emerging luminescent magnetic material

(Kurungottu *et al*., 2024; Lim *et al*., 2015; Makadia & Siegel, 2011; Salimi *et al*., 2025; K. Wang *et al*., 2021).

Multidisciplinary scientists have been particularly interested in carbon quantum dots (CQDs) due to their small size, excellent photostability, intense fluorescence, high water solubility, non-toxicity, and outstanding biocompatibility. CQDs are a promising alternative for magnetic metal-based bioimaging applications due to their superior properties (Das *et al*., 2023; Mmelesi *et al*., 2024; Molaei, 2019; Yadav *et al*., 2023). However, combining $Fe_3O_4$ with CQD can reduce CQD luminescence intensity. $Fe_3O_4$ quenches CQD luminescence, and CQDs interact readily with their environment when applied to the human body as bioimaging materials, thereby reducing their luminescence intensity. Therefore, a polymer must be added to the surface of $Fe_3O_4$@CQD nanocomposites without affecting their dispersibility to increase their luminescence. Polylactic acid (PLA) is a biodegradable polymer.

To increase luminescence intensity while preserving water dispersibility, $Fe_3O_4$@CQD nanocomposites can be coated with PLA on their exterior for use as bioimaging materials (Osaci & Cacciola, 2020; Zhao *et al*., 2020). PLA is not only biodegradable but also resistant to enzymatic degradation over an extended period. Furthermore, throughout the coating and application processes, the $Fe_3O_4$ particles are shielded from high temperatures by PLA's remarkable thermal stability. Additionally, magnetite's hydrophobic properties prevent clumping and unintended interaction with bodily fluids. The quality of the images in the bioimaging process is ensured by PLA's good optical qualities, which do not interfere with the magnetite signal (Zaaba & Jaafar, 2020).

PLA-coated $Fe_3O_4$@CQD nanocomposites with a core-shell structure were synthesized for this investigation. Hydrothermal synthesis was used to create CQDs. Nanocomposites of $Fe_3O_4$@CQD were synthesized using the coprecipitation technique. $Fe_3O_4$@CQD was coated with PLA via sonication. PLA-coated $Fe_3O_4$@CQD nanocomposites are expected to exhibit improved luminescence characteristics and surface stability. These physicochemical properties may make the material a potential candidate for further investigation in bioimaging-related applications. However, a biological evaluation is required to determine its biocompatibility and actual suitability for biomedical use.

## 2. Methodology

### *2.1 $Fe_3O_4$ Synthesis*

Nanoparticles of $Fe_3O_4$ were prepared via a coprecipitation method under an air atmosphere. $Fe_3O_4$ nanoparticles were synthesized with a molar ratio of $Fe^{3+}$: $Fe^{2+}$ = 2:1 as follows: dissolve 2.02725 g of $FeCl_3 \cdot 6H_2O$ and 1.0425 g of $FeSO_4 \cdot 7H_2O$, and use 30 mL of distilled water heated to 60°C on a hot plate. A black precipitate formed when the mixture was stirred for three hours with a magnetic stirrer, and 30 mL of $NH_4OH$ solution was gradually added until the pH reached 11 (Astuti et al., 2023). A permanent magnet was used to facilitate the precipitation of $Fe_3O_4$. The precipitate was dried in a furnace for five hours at 150°C after being washed three times with distilled water. The precipitate was dried and then milled into a fine powder of $Fe_3O_4$.

### *2.2 Carbon Quantum Dots Synthesis*

Two grams of Sappan wood sample (*Caesalpinia sappan L.)* are dissolved in 30 mL of distilled water and stirred for 30 minutes to hydrothermally produce CQD. To create Sappan wood extract, the mixture was filtered through filter paper. The hydrothermal procedure involves heating the Sappan wood extract solution to 150 °C for eight hours in an autoclave.

### *2.3 $Fe_3O_4$@CQD Nanocomposite Synthesis*

After dissolving 0.4 g of $Fe_3O_4$ powder in 20 mL of CQD solution, the mixture was sonicated for 30 minutes to form $Fe_3O_4$@CQD. The sonication process aims to disintegrate the molecules into nanometer-sized particles. To separate the sediment and liquid, the sonicated solution was centrifuged for 20 minutes at 4500 rpm. The centrifuged sediment was dried for two hours at 50°C in a furnace.

### *2.4 $Fe_3O_4$@CQD Nanocomposite Coating with PLA*

As much as 0.1 g of $Fe_3O_4$@CQD nanocomposite was mixed with 5 mL of a polylactic acid-dimethyl sulfoxide solution at 2% (w/w) and stirred until homogeneous under ambient atmosphere. The homogeneous mixture was then added to 50 mL of distilled water supplemented with 5 mL of a 5% PVA solution as a stabilizer and sonicated for 30 minutes. The sonicated solution was then centrifuged for 30 minutes at 4000 rpm. The centrifugation process

produced sediment and liquid. Next, the sediment from the centrifugation was dried in an oven at 50°C for 4 hours. The synthesis of the following sample was carried out in the same manner, with variations in polylactic acid concentrations of 0.5%, 5%, 7%, and 10%. Furthermore, the sample, in the form of a dry powder, was characterized using XRD, FTIR, UV fluorescence, zeta potential, and SEM-EDX.

*2.5 Characterization Methods*

This work reports the characterization of the $Fe_3O_4$@CQD-PLA nanocomposite, including crystal structure analysis using an XRD instrument (Bruker D8 Advance). Using Cu-Kα radiation (λ=1.5406 Å) of $10°<2\theta<100°$ with increments of 0.02°, the diffractogram was produced. SEM (HITACHI FLEXEM 1000) was used to examine the samples' morphology, and fluorescence microscopy (Zeiss Axio Imager A2 and EVOS M7000) was used to examine the fluorescence analysis. FTIR (Nicolet iS50) for identifying functional groups. With a resolution of 1.29 $cm^{-1}$, these measurements were carried out in the frequency range of 450 $cm^{-1}$–4000 $cm^{-1}$.

## 3. Results and Discussion

*3.1 Colloids of CQD and $Fe_3O_4$@CQD Nanocomposites.*

CQD colloids before and after UV irradiation are shown in Figure 1. Figure 1 shows that CQD emits green light luminescence under UV illumination.

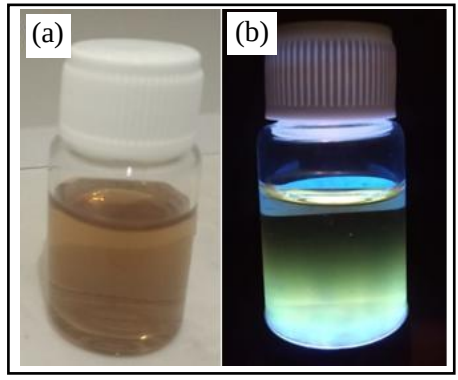


Figure 1. The colloid of CQD: CQD before UV illumination (a), CQD under UV illumination (b)

The emitted luminescence indicates the formation of CQDs with a reasonably uniform distribution. Uniform distribution is also confirmed by the TEM images shown in Figure 2.

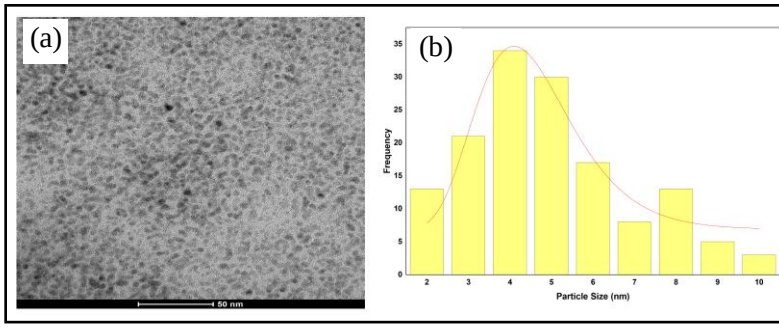


Figure 2. TEM image of CQD colloid (a), particle size distribution of CQD colloid (b)

Figure 2a is a TEM image of CQD colloids, while Figure 2b is a histogram for particle size distribution. The measurement results indicate that the particle size distribution is primarily characterized by particles ranging from 2 to 4 nm.

*3.2 X-ray Diffraction (XRD) Characterization*

Finding the crystalline substance and crystal size of PLA-coated $Fe_3O_4$ @CQD and $Fe_3O_4$ is the aim of the XRD measurement. The XRD readings were analyzed using OriginPro 2025. The material's X-ray diffraction pattern is displayed in Figure 3. Figure 3 shows a clear and distinct diffraction pattern from the XRD analysis of the pure $Fe_3O_4$ sample. The dominance of crystal orientation in the (311) plane was demonstrated by the identification of substantial peaks at 2θ angles of approximately 30°, 35°, 43°, 53°, 57°, 63°, and 90°, with the most prominent peak at 35°. The material's stable crystal structure and good phase purity are confirmed by the pattern's fit to the standard reference for $Fe_3O_4$ structure (Sahebalzamani *et al.*, 2020). According to the computational results, the crystal size is 25.5 nm, placing it in the nanocrystalline group. The sharp peaks also demonstrate the crystals' consistent alignment.

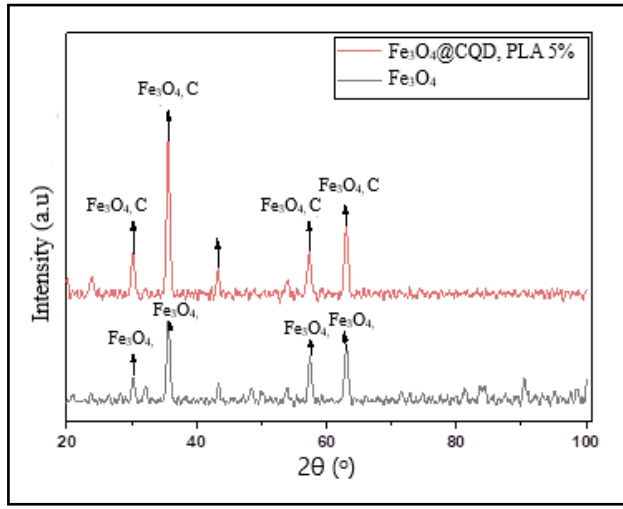


Figure 3. XRD patterns of $Fe_3O_4$ and $Fe_3O_4$@CQD, PLA 5%

When $Fe_3O_4$ was combined with carbon quantum dots (CQD) and coated with PLA, the distinctive diffraction pattern of $Fe_3O_4$ was still evident at the same angular positions as seen in Figure 3, specifically at 30°, 35°, 57°, and 63°. The intensity of the resulting diffraction peak, which exceeds the initial level, indicates good crystallinity. A high diffraction intensity indicates that the modification process has not compromised the $Fe_3O_4$ crystal structure. The observed crystal size, approximately 25.63 nm, indicates that the coating does not prevent crystal formation and continues to produce nanoscale particles.

Furthermore, the presence of PLA in a semi-crystalline form is indicated by a strong diffraction peak at approximately $2\theta = 23°$. This suggests that PLA is evenly distributed across the particle surface, forming a sufficiently regular structure for XRD to detect. The amorphous CQD may reduce the diffraction background, even though it does not yield a distinct diffraction peak. The XRD results, as shown in Figure 3, demonstrate that the crystalline structure of $Fe_3O_4$ remains stable when mixed with CQD and PLA, as evidenced by the semi-crystalline contribution of PLA and the crystal size falling within the nanoscale range. The synthesis process successfully produced a small-particle-size, stable, and uniformly distributed composite material, promising for various nanomaterial-based applications.

### *3.3 FTIR Characterization*

$Fe_3O_4$@CQD nanocomposite material without PLA coating and coated with PLA at concentration changes of 2%, 5%, 7%, and 10% was subjected to FTIR analysis. This work aims to identify the functional groups in $Fe_3O_4$@CQD nanocomposites, both coated and uncoated, with PLA. Wavenumbers ranging from 450 $cm^{-1}$ to 4000 $cm^{-1}$ are used in FTIR spectroscopy. Transmission peaks corresponding to the vibrational energy depicted in Figure 4 are observed in the test results.

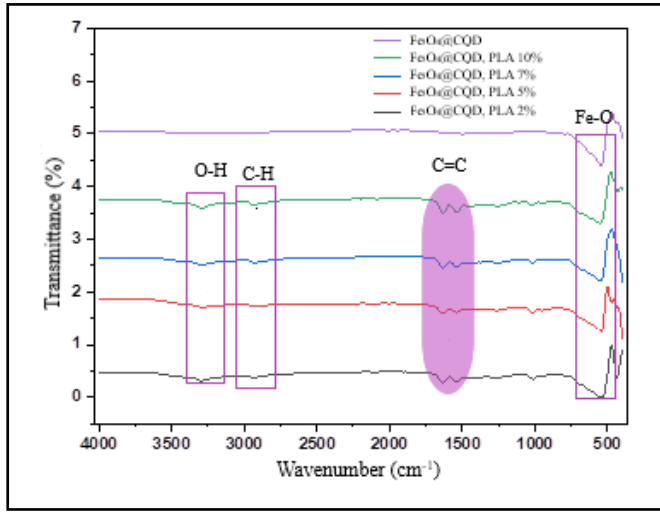


Figure 4. The FTIR spectra of $Fe_3O_4$@CQD

The presence of the $Fe_3O_4$ structure and other functional groups is confirmed by several significant peaks in the FTIR spectrum of $Fe_3O_4$@CQD without coating, as shown in Figure 4. As is common for $Fe_3O_4$, the peak at 545.45 $cm^{-1}$ is ascribed to Fe-O stretching vibrations. Furthermore, the presence of the $Fe_3O_4$ phase is supported by a peak at 435.22 $cm^{-1}$, attributed to Fe-O vibrations (Syihabuddin, 2024). In Carbon Quantum Dots (CQD), aromatic C=C stretching vibrations are linked to another notable peak at 1494.76 $cm^{-1}$. On the other hand, the presence of C-O groups of carboxylates or esters is indicated by the carbonyl signal at 1296.28 $cm^{-1}$. The broad peak at 3167.94 $cm^{-1}$ indicates the presence of O-H groups, which could arise from adsorbed water or hydroxyl groups on the CQD surface (Cruz *et al*., 2019).

The FTIR spectra showed changes after coating with 2% PLA. The distinctive Fe-O peak at 535.02 $cm^{-1}$ remains visible despite the coating, indicating that the $Fe_3O_4$ structure is still there. An interaction between the carbonyl groups of CQD and PLA is suggested by the C=C double bond in the carbonyl signal at 1633.64 $cm^{-1}$. The PLA chain's aliphatic C-H stretching vibrations are at 2931.46 $cm^{-1}$. The broad O-H peak at 3292.59 cm-$^{1}$, which remains discernible but is weaker than in the uncoated sample, indicates that some hydroxyl groups have interacted with the PLA. A different study suggests that changes in the O-H and C=O peak intensities after polymer coating may indicate interactions between the magnetic nanoparticles and the polymer coating (Lao *et al*., 2021).

The absorption peaks were not substantially altered by the additional PLA, particularly at concentrations of 5%, 7%, and 10%. The Fe-O peak, still discernible at roughly 540.95 cm-1 but continuing to wane relative to the 2% sample, indicated that the PLA layer had begun to coat a larger portion of the $Fe_3O_4$ surface. Additionally, the C-O stretching peak at 1260.53 $cm^{-1}$ and the C-H stretching peak at 2930.11 $cm^{-1}$ both show an increase in intensity. Furthermore, the presence of C-O-C groups in the PLA chain is indicated at the beginning of a peak at 1015.27 $cm^{-1}$. The absorption peaks were not substantially altered by increasing amounts of PLA (5%, 7%, and 10%).

### *3.4 Zeta Potential Characterization*

To evaluate the effect of PLA coating on the surface charge and colloidal stability of $Fe_3O_4$@CQD nanocomposites, zeta potential measurements were performed using water as the dispersing medium (Figure 5). Zeta potential measurements were performed using water as the dispersing medium. According to the measurement results graph, the zeta potential of $Fe_3O_4$@CQD without PLA is -52.5 mV, while the zeta potentials of $Fe_3O_4$@CQD with 0.5% PLA, 2% PLA, and 7% PLA are -15.4 mV, -32.2 mV, and -31.3 mV, respectively. Zeta potential measurements indicate that the concentration and presence of PLA as a coating material substantially affect the surface charge of $Fe_3O_4$@CQD particles. The PLA-free sample exhibited a maximum zeta potential of -52.5 mV and a highly electrostatically stable colloidal structure. According to Öztürk *et al*. (2024) and Pochapski *et al*. (2021), it is commonly accepted that potential zeta values $|\zeta| \geq 30$ mV (positive or negative) are adequate to maintain colloidal stability through repulsive interactions between particles that prevent agglomeration.

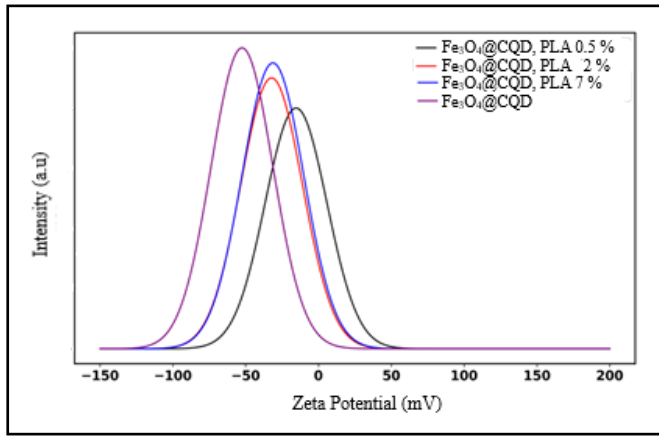


Figure 5. Zeta potential test results of $Fe_3O_4$@CQD-PLA

The zeta potential increased to -32.2 mV and -31.3 mV in the samples containing 2% and 7% PLA, although they stayed within the stable range. The slight increase shows that the PLA layer maintains sufficient repulsive force to prevent aggregation. However, the zeta potential increased sharply to -15.4 mV at 0.5% PLA concentration, indicating inadequate colloidal stability. This finding suggests that, unlike higher PLA concentrations, which can lead to polymer buildup or an uneven structure, lower PLA concentrations facilitate the formation of a more uniform layer and effectively neutralize surface charges (Da Silva *et al*., 2019; Ekinci *et al*., 2022). The zeta potential (ζ-potential) value of each sample is shown in Table 1.

Table 1. Zeta potential (ζ-potential) value of each sample

| Sample-PLA concentrations | ζ-potential |
|---|---|
| $Fe_3O_4$ @CQD | -52.5 mV |
| $Fe_3O_4$ @CQD-PLA (0.5 %) | -15.4 mV |
| $Fe_3O_4$ @CQD-PLA (2 %) | -32.2 mV |
| $Fe_3O_4$ @CQD-PLA (7 %) | -31.3 mV |

Coating with PLA decreases the zeta potential, indicating increased ionic strength and aggregation. However, the decrease in the zeta potential value in 2% PLA, which is -32.2 mV, is still classified as a stable colloid with low-moderate ionic strength. One of the tested formulations, the 2% PLA sample, had a zeta potential of −32.2 mV, which falls within the range reported for relatively stable colloidal systems. Thus, the 2% PLA formulation exhibited

good surface charge properties under the experimental conditions of the present study.

The body may circulate more slowly and interact less adversely with blood proteins if the zeta potential is higher. This advantage may make high zeta potential (such as -32.2 mV) more biocompatible than low zeta potential ones in biological imaging or drug administration applications (Öztürk *et al*., 2024; Serrano-Lotina *et al*., 2023). In certain situations, a moderate negative charge (~–30 mV) may be more advantageous than a very low charge if the particles are intended for in vivo imaging (enhanced circulation and reduced nonspecific binding), provided that stability is maintained. However, these results are insufficient to establish biological compatibility or suitability for in vivo applications, and further optimization and testing are needed.

*3.5 UV Fluorescence Characterization*

UV fluorescence was used to characterize the $Fe_3O_4$@CQD samples coated with PLA at 0.5%, 2%, and 7%, as well as those without PLA. UV fluorescence spectra of $Fe_3O_4$/CQD nanocomposites without and with PLA variations were measured in the wavelength range of 400-650 nm, as shown in Figure 6. The excitation wavelength used is 300 nm.

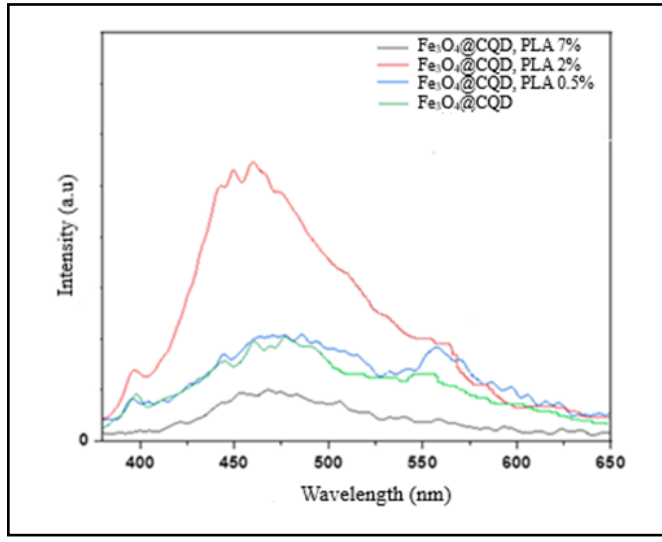


Figure 6. The UV Fluorescence spectra of $Fe_3O_4$@CQD-PLA

The UV fluorescence test revealed a significant increase in the fluorescence emission intensity of $Fe_3O_4$@CQD nanocomposites following PLA coating, particularly at 2% concentration. Increased fluorescence intensity indicates that the PLA coating effectively reduces quenching effects, usually caused by surface defects or interactions with oxygen, by forming a surface shield that inhibits non-radiative processes and maintains the photoluminescence stability of the CQDs. Improved homogeneity and dispersion of nanoparticles in the fluid may contribute to this rise in fluorescence intensity by enhancing the efficacy of light-particle surface contact. The highest observed fluorescence intensity was obtained for the sample containing 2% PLA. This result suggests that, under the experimental conditions used in this study, 2% PLA provided the most favorable fluorescence response among the tested concentrations. The increase in fluorescence may be associated with surface passivation and reduced quenching; however, further experiments are required to confirm the underlying mechanism (Kato *et al*., 2022)

Since the coating is not uniformly applied, protection against CQD is subpar at 0.5% PLA, and the increase in intensity is negligible. Conversely, at a 7% PLA concentration, the fluorescence intensity decreases due to optical resistance or self-absorption resulting from the excessive thickness of the PLA layer. To mitigate adverse impacts on photoluminescence, the PLA coating not only enhances fluorescence stability but also improves coating concentration and uniformity (Khalaf *et al*., 2024). Crystalline CQDs are more vulnerable to self-quenching events caused by surface contacts at short distances in the solid state because they have a higher fraction of $sp^2$ domains than amorphous CQDs. Nevertheless, even in the solid state, surface passivation using PLA chains ensures a superior emission profile for CQDs. Superior emission is attributed to the outstanding dispersion of CQDs within the PLA solid matrix, facilitated by the presence of a polymer shell at their surface, which significantly reduces π-π core interactions (Mauro *et al.*, 2024).

### *3.6 SEM EDX Characterization*

A scanning electron microscope (SEM) was used to evaluate the surface morphology, shape, and particle size of the $Fe_3O_4$@CQD and $Fe_3O_4$@CQD PLA 2% sample. Figure 7a and 7b show the SEM image of the $Fe_3O_4$@CQD and mapping. The SEM image of $Fe_3O_4$/CQD reveals an irregular morphology with a tendency to form agglomerates. The observed agglomeration is likely attributable to inter-particle interactions among $Fe_3O_4$ particles—specifically magnetic dipole-dipole interactions—as well as surface interactions occurring during the synthesis and drying processes. A distribution of small granules is

visible on the surface of the agglomerates, indicating the formation of $Fe_3O_4$@CQD nanocomposites. EDX mapping data (shown in Figure 8a) indicate Fe, O, and C contents of 70.45%, 20.10%, and 9.45%, respectively.

Figure 7c shows the SEM image of the $Fe_3O_4$@CQD-PLA 2% sample at 1,000× magnification, whereas Figure 7d shows the image at 5,000× magnification. The spherical, irregular shape of the particles produces large agglomerates at 1,000× magnification. Due to interparticle attraction, magnetic nanoparticles such as Fe3O4 often agglomerate (Yew *et al*., 2020). At 5,000× magnification, the rough and porous particle surfaces clearly indicate the presence of a PLA polymer coating, despite the distribution's apparent irregularity. The particle morphology, consisting of a collection of nano- to submicron-sized particles, is further emphasized by the 5,000× magnification image. The agglomeration phenomenon is closely related to the synthesis parameters and synthesis method used. These synthesis parameters can increase atomic mobility and particle surface energy, thereby promoting coalescence and particle growth during synthesis, particularly in magnetic-based materials such as $Fe_3O_4$ used in this study.

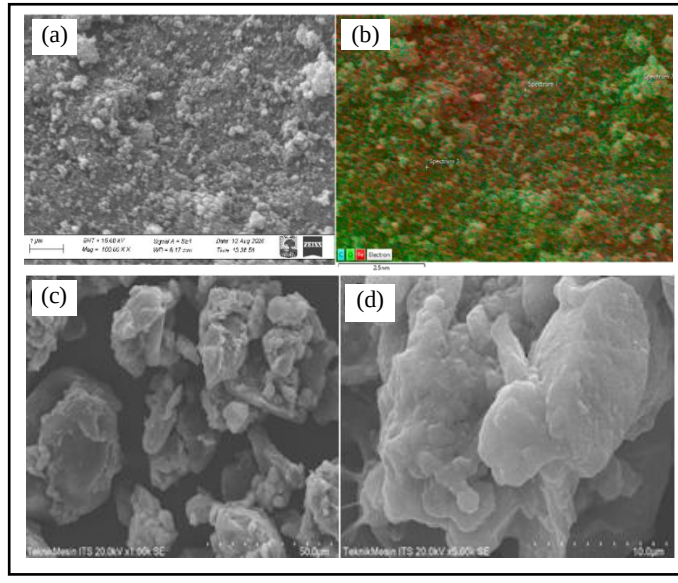


Figure 7. SEM results of $Fe_3O_4$@CQD (a)-(b), $Fe_3O_4$@CQD-PLA 2%: 1,000× magnification (c), 5,000× magnification (d)

To ascertain the distribution of constituent elements in the PLA-coated $Fe_3O_4$@CQD sample, EDX Mapping characterization was also carried out. The presence and distribution of the elements Fe, O, and C on the particle surface are verified using this method in conjunction with SEM analysis. This elemental mapping, which reveals the presence of carbon and polymer layers, validates the efficacy of the material production process. The $Fe_3O_4$@CQD-PLA 2% sample contains three major elements: iron (Fe), oxygen (O), and carbon (C), as indicated by the EDX analysis results displayed in Figure 8b. Their relative weight compositions are 57.57%, 26.84%, and 15.59%. The rise in the amounts of O and C in the $Fe_3O_4$@CQD-PLA shows that PLA is adding to the nanocomposite.

The EDX results for this sample are semi-quantitative, so the elemental percentage values obtained serve only to verify the relative composition, not for an absolute quantitative analysis. The formation of the $Fe_3O_4$@CQD nanocomposite with 2% PLA, with most of the nanocomposite coated with PLA, was confirmed by SEM and EDX data (Salimi *et al*., 2025).

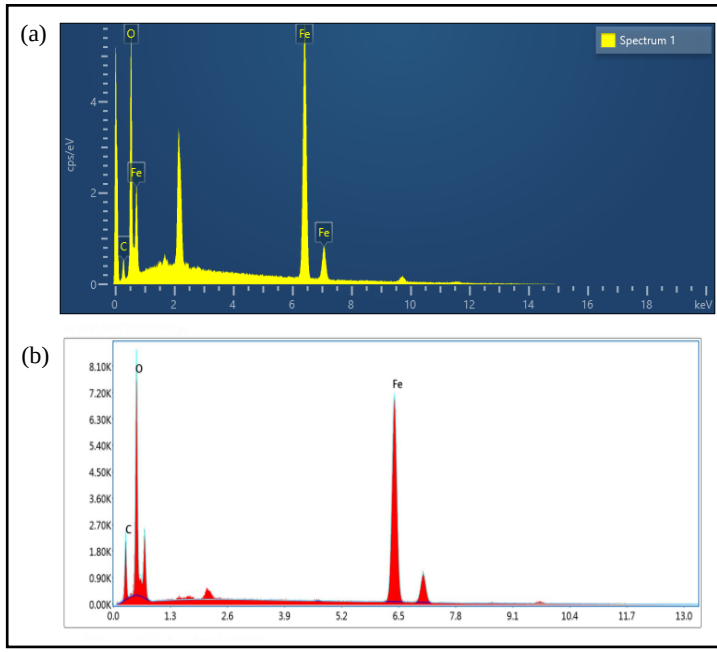


Figure 8. EDX results of $Fe_3O_4$@CQD (a), $Fe_3O_4$@CQD-PLA 2% (b)

Additional modifications to the coating ratio, sonication time, and synthesis technique are necessary, as the development of agglomeration and an uneven

surface suggests the coating process was not performed consistently. The SEM observations indicate that the 2% PLA-coated $Fe_3O_4$@CQD sample exhibits particle agglomeration and a non-uniform surface morphology. Although the surface characteristics are consistent with a polymer coating, the coating does not completely prevent particle aggregation. The EDX mapping confirms the presence of Fe, O, and C in the sample, supporting the formation of the $Fe_3O_4$@CQD-PLA composite. Therefore, the SEM-EDX results support the formation of a PLA-containing nanocomposite but also indicate that further optimization of the coating ratio, sonication conditions, and synthesis parameters is needed to improve surface uniformity and reduce agglomeration (Fattahi Nafchi *et al*., 2022; Osaci & Cacciola, 2020).

## 4. Conclusions and Recommendations

XRD and FTIR studies have demonstrated the successful completion of $Fe_3O_4$@CQD coating with PLA. FTIR results at PLA concentrations of 2%, 5%, 7%, and 10% indicate the formation of a PLA coating on $Fe_3O_4$@CQD, while XRD results for the $Fe_3O_4$@CQD sample with 5% PLA confirm that no change in the crystal structure of $Fe_3O_4$ occurred. The 2% PLA formulation also exhibited a zeta potential of −32.2 mV, indicating relatively favorable colloidal stability under the experimental conditions. However, SEM analysis revealed particle agglomeration and a non-uniform surface morphology, indicating that further optimization of the coating process is required. The potential studies of zeta further demonstrate that PLA's efficacy as a dispersant is significantly influenced by concentration and synthesis techniques. Overall, the physicochemical results suggest that the $Fe_3O_4$@CQD-PLA nanocomposite, particularly at 2% PLA, has potential for further investigation in bioimaging-related applications. Further studies involving cytotoxicity, biocompatibility and imaging performance are necessary before its biomedical applicability can be established.

## 5. Acknowledgment

This research is funded by the RKAT of the Faculty of Mathematics and Natural Sciences, Andalas University, by the BATCH II research contract of

the Basic Research scheme, Number: 09/UN.16.03.D/PP/FMIPA/2024, Fiscal Year 2024.

## 6. References

Astuti, Arief, S., Muldarisnur, M., & Zulhadjri. (2024). Green synthesis of $Fe_3O_4$@CDs nanocomposites and its performance on optical and magnetic properties. *Evergreen*, *11*(2), 673–681. https://doi.org/10.5109/7183339

Astuti, Arief, S., Muldarisnur, M., Zulhadjri, & Usna, S.R.A. (2023). Enhancement in photoluminescence performance of carbon-based $Fe_3O_4$@ZnO–C nanocomposites. *Vacuum*, 211, 111935. https://doi.org/10.1016/j.vacuum.2023.111935

Cruz, R.A.T., Soriano, A.N., De Yro, P.A.N., Quiachon, G.M.O., Emolaga, C.S., Ysulat, M.L.M., Bigol, U.G., & Basilia, B.A. (2019). Functionalized carbon-based quantum dots: Optical characterization and potential application as bio-fluorophore. *IOP Conference Series: Materials Science and Engineering*, *559*(1), 012003. https://doi.org/10.1088/1757-899X/559/1/012003

Das, S., Mondal, S., & Ghosh, D. (2023). Carbon quantum dots in bioimaging and biomedicines. *Frontiers in Bioengineering and Biotechnology*, *11*, 1–22. https://doi.org/10.3389/fbioe.2023.1333752

Fattahi Nafchi, R., Ahmadi, R., Heydari, M., Rahimipour, M.R., Molaei, M.J., & Unsworth, L. (2022). In vitro study: synthesis and evaluation of $Fe_3O_4$/CQD magnetic/fluorescent nanocomposites for targeted drug delivery, MRI, and cancer cell labeling applications. *Langmuir*, *38*(12), 3804–3816. https://doi.org/10.1021/acs.langmuir.1c03458

Kato, R., Uesugi, M., Komatsu, Y., Okamoto, F., Tanaka, T., Kitawaki, F., & Yano, T. (2022). Highly stable polymer coating on silver nanoparticles for efficient plasmonic enhancement of fluorescence. *ACS Omega*, *7*(5), 4286–4292. https://doi.org/10.1021/acsomega.1c06010

Khalaf, M.M., Gouda, M., Hamdalla, T.A., Taleb, M.F.A., & El-Lateef, H.M.A. (2024). Development of carbon dots-immobilized fluorescent polylactic acid hydrogel ink toward security authentication. *Polymer Engineering & Science*, *64*(9), 4196–4209. https://doi.org/10.1002/pen.26841

Kurungottu, P., Thomas, M. Ben, Lalitha, M.M., Ganesh, P., Gnanadhas, D.P., Chakravortty, D., Raichur, A. M., & Kurapati, R. (2024). Biodegradable

nanocomposite of ZnS(Mn) quantum dots immobilized graphene oxide for bioimaging applications. *Nanotheranostics*, *8*(2), 150–162. https://doi.org/10.7150/ntno.87536

Lim, S.Y., Shen, W., & Gao, Z. (2015). Carbon quantum dots and their applications. *Chemical Society Reviews*, *44*(1), 362–381. https://doi.org/10.1039/C4CS00269E

Makadia, H.K., & Siegel, S.J. (2011). Poly lactic-co-glycolic acid (PLGA) as biodegradable controlled drug delivery carrier. *Polymers*, *3*(3), 1377–1397. https://doi.org/10.3390/polym3031377

Mauro, N., Calabrese, G., Sciortino, A., Rizzo, M.G., Messina, F., Giammona, G., & Cavallaro, G. (2024). Microporous fluorescent poly(D,L-lactide) acid–carbon nanodot scaffolds for bone tissue engineering applications. *Materials*, 17(2), 449. https://doi.org/10.3390/ma17020449

Mmelesi, O.K., Mguni, L.L., Li, F.T., Nkosi, B., & Liu, X. (2024). Recent development in fluorescent carbon quantum dots-based photocatalysts for water and energy applications. *Materials Science in Semiconductor Processing*, *181*, 108661. https://doi.org/10.1016/j.mssp.2024.108661

Molaei, M.J. (2019). Carbon quantum dots and their biomedical and therapeutic applications: A review. *RSC Advances*, *9*(12), 6460–6481. https://doi.org/10.1039/c8ra08088g

Osaci, M., & Cacciola, M. (2020). Influence of the magnetic nanoparticle coating on the magnetic relaxation time. *Beilstein Journal of Nanotechnology*, *11*, 1207–1216. https://doi.org/10.3762/bjnano.11.105

Öztürk, K., Kaplan, M., & Çalış, S. (2024). Effects of nanoparticle size, shape, and zeta potential on drug delivery. *International Journal of Pharmaceutics*, *666*, 124799. https://doi.org/10.1016/j.ijpharm.2024.124799

Sahebalzamani, H., Mehrani, K., Madaah, H., Hamid, R., & Zare, K. (2020). Effect of synthesis temperature of magnetic–fluorescent nanoparticles on properties and cellular imaging. *Journal of Inorganic and Organometallic Polymers and Materials*, 30, 4597-4605. https://doi.org/10.1007/s10904-020-01720-5

Salimi, S., Motalleb, G., Dehghani, H., Rahdar, A., Dastjerdi, K., Velasco, B., & Taboada, P. (2025). Anticancer effect of tamoxifen and $Fe_3O_4$@SiO2@Cu hybrid NPs on malignant human breast cancer cell (MCF-7). *Journal of Molecular Liquids*, *429*, 127570. https://doi.org/10.1016/j.molliq.2025.127570

Serrano-Lotina, A., Portela, R., Baeza, P., Alcolea-Rodriguez, V., Villarroel, M., & Ávila, P. (2023). Zeta potential as a tool for functional materials development. *Catalysis Today*, *423*, 113862. https://doi.org/10.1016/j.cattod.2022.08.004

Wang, K., Xu, X., Li, Y., Rong, M., Wang, L., Lu, L., Wang, J., Zhao, F., Sun, B., & Jiang, Y. (2021). Preparation of $Fe_3O_4$@chitosan-graphene quantum dots nanocomposites for fluorescence and magnetic resonance imaging. *Chemical Physics Letters*, *783*, 139060. https://doi.org/10.1016/j.cplett.2021.139060

Wang, M., & Deng, M. (2022). Synthesis and characterization of fluorescent magnetic $Fe_3O_4$/CdTe@$SiO_2$-NH-FA nanoprobe. *Materials Letters*, *309*, 131358. https://doi.org/10.1016/j.matlet.2021.131358

Yadav, P.K., Chandra, S., Kumar, V., Kumar, D., & Hasan, S.H. (2023). Carbon quantum dots: Synthesis, structure, properties, and catalytic applications for organic synthesis. *Catalysts*, *13*(2). https://doi.org/10.3390/catal13020422

Yao, L., Wang, Y., Li, Y., Liu, J., & Zhou, X. (2021). Controlled preparation of $Fe_3O_4$/PLA composites and their properties. *Chemical Papers*, 75, 6399–6406. https://doi.org/10.1007/s11696-021-01809-2

Yew, Y.P., Shameli, K., Miyake, M., Ahmad Khairudin, N.B.B., Mohamad, S.E.B., Naiki, T., & Lee, K.X. (2020). Green biosynthesis of superparamagnetic magnetite $Fe_3O_4$ nanoparticles and biomedical applications in targeted anticancer drug delivery system: A review. *Arabian Journal of Chemistry*, *13*(1), 2287–2308. https://doi.org/10.1016/j.arabjc.2018.04.013

Zaaba, N.F., & Jaafar, M. (2020). A review on degradation mechanisms of polylactic acid: Hydrolytic, photodegradative, microbial, and enzymatic degradation. *Polymer Engineering & Science*, *60*(9), 2061–2075. https://doi.org/10.1002/pen.25511

Zhao, X., Yu, Q., Yuan, J., Thakor, N.V., & Tan, M.C. (2020). Biodegradable rare earth fluorochloride nanocrystals for phototheranostics. *RSC Advances*, *10*(26), 15387–15393. https://doi.org/10.1039/d0ra00760a